Electrostatically Driven Coassembly of a Diblock Copolymer and an Oppositely Charged Homopolymer in Aqueous Solutions

Ilja K. Voets,*,† Stefan van der Burgh,† Bela Farago,‡ Remco Fokkink,† Davor Kovacevic,† Thomas Hellweg,§ Arie de Keizer,† and Martien A. Cohen Stuart†

Laboratory of Physical Chemistry and Colloid Science, Wageningen University, Dreijenplein 6, 6703 HB Wageningen, The Netherlands, Institut Max von Laue−Paul Langevin, F-38042 Grenoble Cedex 9, France, and Physikalische Chemie I, University of Bayreuth, 95440 Bayreuth, Germany

Received June 19, 2007; Revised Manuscript Received August 22, 2007

ABSTRACT: Electrostatically driven coassembly of poly(acrylic acid)-*block*-poly(acrylamide), PAA-*b*-PAAm, and poly(2-methylvinylpyridinium iodide), P2MVP, leads to formation of micelles in aqueous solutions. Light scattering and small angle neutron scattering experiments have been performed to study the effect of concentration and length of the corona block (N_{PAAm} = 97, 208, and 417) on micellar characteristics. Small angle neutron scattering curves were analyzed by generalized indirect Fourier transformation and model fitting. All scattering curves could be well described with a combination of a form factor for polydisperse spheres in combination with a hard sphere structure factor for the highest concentrations. Micellar aggregation numbers, shape, and internal structure are relatively independent of concentration for C_p < 23.12 g L^{-1}. The Guinier radius, average micellar radius, hydrodynamic radius, and polydispersity were found to increase with increasing N_{PAAm}. Micellar mass and aggregation number were found to decrease with increasing N_{PAAm}.

Introduction

Micelles formed by the electrostatically driven assembly of oppositely charged components are relatively novel particles in the field of "self"-assembly. The resulting particles are termed complex coacervate core micelles (C3Ms), polyion complex (PIC) micelles, block ionomer complex (BIC) micelles, or interpolyelectrolyte complexes (IPEC). Strictly speaking, the correct term would be coassembly, as self-assembly excludes structures consisting of multiple components. In this study, we focus on C3Ms consisting of a neutral−ionic block copolymer and a polyelectrolyte with an opposite charge sign. A sketch of such a system is presented in Figure 1.

The novelty of C3Ms lies in the fact that the separate components are hydrophilic, i.e., no micellization occurs in solutions of single components. Yet, when mixed under appropriate conditions (pH, ionic strength, mixing ratio), C3Ms may form. A number of publications on this type of assembly can be found in the literature. The radius of the micelles is generally of the order of several tens of nanometers and electrophoretic mobility measurements indicate that the micelles carry no excess charge. An important driving force for aggregation is the entropy gain associated with the release of counterions from the polyelectrolyte double layers. Hence, C3Ms dissociate above a critical ionic strength when charges are highly screened. The micelles form in a rather small compositional window around the so-called preferred micellar composition, PMC, which corresponds to a mixing ratio of 1:1 as expressed in chargeable monomers for equal charge densities of the polyelectrolyte blocks. The following speciation as a function of mixing ratio has been proposed.[1] When the composition of the system is exactly at the PMC, the system exclusively forms micelles. When the composition is chosen somewhat away from the PMC, coexistence between soluble complex particles (i.e., small, soluble complexes consisting of a few polymers) and micelles occurs. Further away from the PMC, the micelles disappear altogether and soluble complex particles coexist with free polymer molecules.

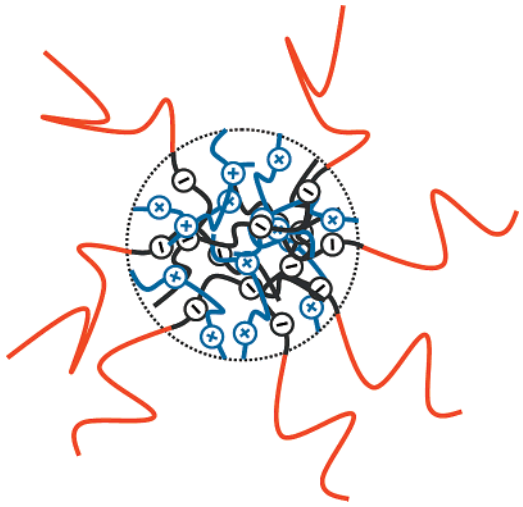

Figure 1. Complex coacervate core micelle. The micellar core consists of the oppositely charged polyelectrolyte blocks PAA and P2MVP, whereas the corona consists of neutral PAAm blocks. Both core and corona are highly water-swollen.

This paper describes light and small angle neutron scattering experiments on C3Ms consisting of poly(acrylic acid)-*block*-poly(acrylamide), PAA-*b*-PAAm, and poly(2-methylvinylpyridinium iodide), P2MVP, intended to study the effect of concentration and polymerization degree of the corona block (N_{PAAm} = 97, 208, and 417) on micellar characteristics, such as shape, mass, aggregation number, radius of gyration, and internal structure. To the best of our knowledge, this is the first SANS study on micelles consisting of a neutral−ionic diblock copolymer and an oppositely charged homopolymer. Closely

* Corresponding author. E-mail: ilja.voets@wur.nl.
† Wageningen University.
‡ Institut Max von Laue−Paul Langevin.
§ University of Bayreuth.

10.1021/ma071356z CCC: $37.00
Published on Web 10/18/2007

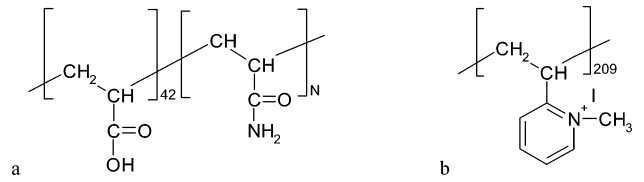

Figure 2. Chemical structure of (a) poly(acrylic acid)-*block*-poly(acrylamide), PAA_{42}-*b*-$PAAm_N$ (N_{PAAm} = 97, 208, and 417) and (b) poly(2-methylvinylpyridinium iodide), $P2MVP_{209}$. The numbers beside the brackets denote the degree of polymerization.

related are SANS studies on mixed micelles consisting of a neutral−ionic block copolymer and a multivalent ion[2,3] or oppositely charged surfactant micelles.[4,5] Berret et al. have published several articles on such systems, incorporating the same PAA-*b*-PAAm diblock copolymers as in this study.[3−5] For mixed polymer/surfactant micelles, it was found that the aggregation number expressed as the number of diblock copolymers per micelle could be as high as 100−250 and that the surfactant micelles keep their micellar structure within the larger structure. The core thus consists of an ensemble of spherical surfactant micelles that are interconnected by the poly(acrylic acid) blocks from the diblock copolymer. The typical distance between the neighboring surfactant micelles showed up as a structure peak at high q values.

C3Ms are expected to have several potential applications. In solution, the micelles can be used for encapsulation, protection, stabilization, and controlled release of virtually any charged species, which may prove to be advantageous in drug delivery, laundry, nanoparticle formation,[6] and food-stuff applications. Substrates, such as silica and polyelectrolyte multilayers, may be rendered antifouling after exposure to C3Ms.[7,8]

Experimental Part

Materials. The diblock copolymers poly(acrylic acid)-*block*-poly(acrylamide), PAA_{42}-*b*-$PAAm_{97}$, PAA_{42}-*b*-$PAAm_{208}$, and PAA_{42}-*b*-$PAAm_{417}$, were a kind gift from Rhodia Chimie, Aubervilliers, France. (The subscripts correspond to the degree of polymerization.) They have been synthesized according to the MADIX process, resulting in an estimated polydispersity index (PDI) ≤ 1.3.[9] The oppositely charged homopolymer poly(2-methylvinylpyridinium iodide), $P2MVP_{209}$ (M_w = 56 000 g mol^{-1}, degree of quaternization ∼70%, PDI = 1.09) has been purchased from Polymer Source Inc., Canada. Chemical structures are depicted in Figure 2.

Stock solutions of P2MVP (38 g L^{-1}) and PAA-*b*-PAAm (25−38 g L^{-1}) were prepared in Milli-Q water (light scattering-titration) or D_2O (99.9% isotopic purity, Isotec Inc., Miamisburg, OH) to which $NaNO_3$ (J. T. Baker Chemicals, Deventer, The Netherlands) was added to obtain a final concentration of 50 mM. The pH of the stock solutions was adjusted with 1 M NaOH/HNO_3 (Merck, Darmstadt, Germany) or NaOD/DNO_3 to obtain pH = 7 for both solutions. All polymers and other chemicals were used as received, without further purification.

Light Scattering-Titrations (LS-T). Details of the experimental setup and data analysis have been reported previously.[10] Results are typically given as pH, total light scattering intensity, $I_{90°}$, and hydrodynamic radius, $R_{h,\ 90°}$, at a scattering angle of 90° as a function of the mixing fraction, f_+. The mixing fraction is defined as the ratio between the number of positively chargeable monomers (i.e., quaternized and nonquaternized monomers) and the sum of the numbers of positively and negatively chargeable monomers, i.e.,

$$f_+ = \frac{[n_+]}{[n_+] + [n_-]} \tag{1}$$

The stock solutions were diluted with a $NaNO_3$ solution of equal ionic strength to obtain PAA-*b*-PAAm solutions of 0.5−1 g L^{-1} and P2MVP solutions of 5 g L^{-1}. In the LS-T experiments, PAA-*b*-PAAm solutions were titrated with a concentrated solution of P2MVP to minimize dilution effects. The LS-T experiments were performed to determine the PMC, which is assumed to be independent of concentration.

Small Angle Neutron Scattering (SANS). Small-angle neutron scattering experiments were performed at the Institut Max von Laue−Paul Langevin (ILL), Grenoble, France, on the D22 beam line. Two detector distances were chosen, such that a q-range of 0.0029−0.137 Å^{-1} was covered, with an incident wavelength of 0.8 nm and a wave-vector resolution $\Delta q/q$ of 10%. The spectra were treated according to standard ILL procedures, and the scattering cross sections are expressed in cm^{-1}. The temperature was kept constant at 293 K. Micellar solutions have been prepared at the preferred micellar composition, PMC, corresponding to f_+ = 0.50 as determined from the LS-T measurements, at concentrations 1.7−38.24 g L^{-1} in pure D_2O for contrast reasons.

The q-dependence of the scattered intensity can be described according to the general equations[11,12]

$$I(q) = n_{part}(\rho_{part} - \rho_{solv})^2 V_{part}{}^2 P(q) S(q) \tag{2}$$

and

$$I(q) = 4\pi \int_0^\infty p(r) \frac{\sin(qr)}{qr}\, dr \tag{3}$$

with the particle number density, n_{part}/cm^{-3}, the particle coherent scattering length density, ρ_{part}/cm^{-2}, the solvent coherent scattering length density, ρ_{solv}/cm^{-2}, the particle volume, V_{part}/cm^3, the form factor, $P(q)$, the structure factor, $S(q)$, the pair distance distribution function, p(r)/cm^{-2}, and the magnitude of the scattering vector, q/cm^{-1}, defined as follows

$$q = \frac{4\pi}{\lambda} \sin\left(\frac{\theta}{2}\right) \tag{4}$$

with the wavelength of the incident radiation, λ, and the angle between the scattered and incident beam, θ. Hence, by indirect Fourier transformation of eq 3, one obtains the pair distance distribution function. In this study, p(r) functions were computed using generalized indirect Fourier transformation employing the GIFT software package.[13−15] A hard sphere structure factor (Percus−Yevick closure,[16] averaged structure factor[17]) has been included to describe the scattering curves of the more concentrated samples.

Alternatively, $I(q)$ may be modeled by selecting a particle form and structure factor fit to describe particle shape and interaction as present in the studied system. In this paper, we applied a hard sphere structure factor (Percus−Yevick closure, decoupling approximation using an average particle radius) and a form factor for homogeneous spheres. In the latter, size polydispersity was included via a Gaussian (N_{PAAm} = 97 and 208) and Schulz−Zimm (N_{PAAm} = 417) size distribution, $f(R,\langle R\rangle)$ with the polydispersity index, p_{real}, and the average particle volume, $\langle V_{part}(R)\rangle$ (see Supporting Information).

The forward scattering intensity at q = 0, I_0, can be used to obtain the particle mass, M_{part}/g mol^{-1}, according to

$$I_0 = \frac{M_{part} C_{part} (\rho_{bb} - \rho_{solv})^2 v_0{}^2}{N_A} \tag{5}$$

with the particle weight concentration, C_{part}/g cm^{-3}, the building block (see below for definition) coherent scattering length density, ρ_{bb}/cm^{-2}, the building block specific volume, v_0/cm^3 g^{-1}, and Avogadro's number, N_A/mol^{-1}. The number of PAA_{42}-*b*-$PAAm_N$ polymers, P_{agg}, per particle can now easily be obtained by division of the particle molar mass, M_{part}, by the building block molar mass, M_{bb}.

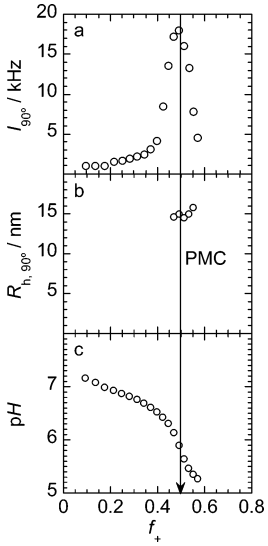

Figure 3. Results of a light scattering titration experiment: (a) light scattering intensity, $I_{90°}$, (b) hydrodynamic radius, $R_{h,90°}$, and (c) pH as a function of f_+. A relatively concentrated $P2MVP_{209}$ solution (~8 g L^{-1}) was titrated with a buret into a dilute PAA_{42}-*b*-$PAAm_{97}$ solution (~0.5 g L^{-1}) in the scattering cell. The initial pH values of the solutions were matched at pH = 7, as was the ionic strength (50 mM $NaNO_3$). The preferred micellar composition, PMC, was determined as the f_+ corresponding to a maximum in $I_{90°}$ and $|dpH/df_+|$. The PMC was assumed to be independent of concentration.

Alternatively, I_0 can also be expressed in the following manner

$$I_0 = \frac{N_A n_{bb}}{P_{agg}} \varphi_{bb,part}{}^2 (\rho_{bb} - \rho_{solv})^2 V_{part}{}^2 \qquad (6)$$

with the building block number density, n_{bb}/mol cm^{-3}, and the building block volume fraction in the particle, $\varphi_{bb,\,part}$. In this way, the $\varphi_{bb,\,part}$ can be obtained by combination of eqs 5 and 6, which is equivalent to stating that

$$\upsilon_0 = \frac{\varphi_{bb,part} V_{part} N_A}{M_{part}} \qquad (7)$$

For the C3Ms in this study, we define a building block as a unit consisting of one diblock copolymer and a corresponding amount of P2MVP groups, i.e., $f_+ = 0.5$. A building block is present P_{agg} times in one particle. The building block for $N_{PAAm} = 97$ equals PAA_{42}-*b*-$PAAm_{97}$ + $P2MVP_{42}$, for $N_{PAAm} = 208$ it is PAA_{42}-*b*-$PAAm_{208}$ + $P2MVP_{42}$, and for $N_{PAAm} = 417$ a building block consists of PAA_{42}-*b*-$PAAm_{417}$ + $P2MVP_{42}$. An overview of the coherent scattering length densities, ρ, specific volume, υ_0, and molecular weights, M_w, of the studied species are given in Table S1 (see Supporting Information).

Results and Discussion

Light Scattering-Titrations (LS-T). Figure 3 shows the results of a light scattering titration where PAA_{42}-*b*-$PAAM_{97}$ was titrated with $P2MVP_{209}$. In analogy to our previous paper,[1] the PMC was found at the maximum in scattered intensity and the maximum in $|dpH/df_+|$; i.e., the PMC is at $f_+ = 0.5$.

Similar experiments were performed for PAA_{42}-*b*-$PAAm_{208}$ and PAA_{42}-*b*-$PAAm_{417}$ (data not shown), and the PMC was always found at $f_+ = 0.5$. Hydrodynamic radii, $R_{h,90°}$, at the PMC are 14.5, 20.2, and 20.4 nm for $N_{PAAm} = 97$, 208, and 417, respectively.

Small Angle Neutron Scattering (SANS). The SANS scattering curves as obtained after data reduction, subtraction of incoherent scattering (both from solvent and hydrogenated polymer units), and division by concentration are presented in Figure 4. The polymer contribution to the incoherent scattering scales linearly with concentration for a given N_{PAAm} (Table 3). Some of the samples exhibit upturns in the first 4−5 points of the scattering curves, which are caused by the presence of a small fraction of larger aggregates, which may be clusters of micelles. All scattering curves appear rather smooth, i.e., distinct features such as form factor minima are absent, which indicates a rather high polydispersity in the systems.

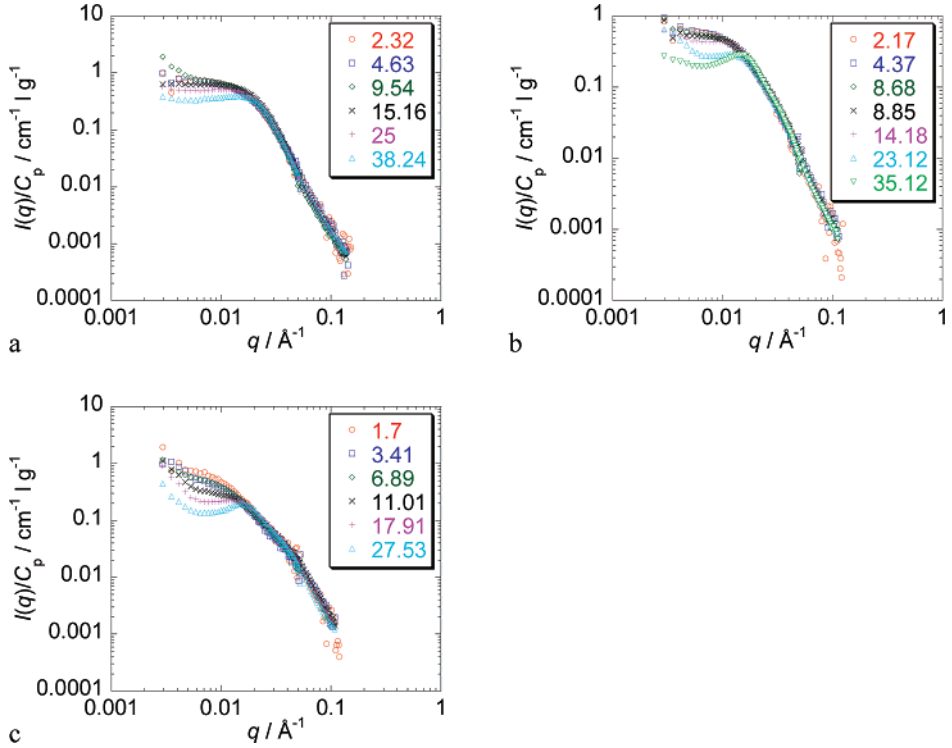

Figure 4. $I(q)/C_p$ (cm^{-1} L g^{-1}) versus q/$Å^{-1}$ for C3Ms of $P2MVP_{209}$ and (a) PAA_{42}-*b*-$PAAm_{97}$ (2.32 g $L^{-1} \le C_p \le$ 38.24 g L^{-1}), (b) PAA_{42}-*b*-$PAAm_{208}$ (2.17 g $L^{-1} \le C_p \le$ 35.12 g L^{-1}), and (c) PAA_{42}-*b*-$PAAm_{417}$ (1.70 g $L^{-1} \le C_p \le$ 27.53 g L^{-1}). Scattering curves have been corrected for incoherent scattering, due to solvent and hydrogenated polymer segments, and divided by C_p.

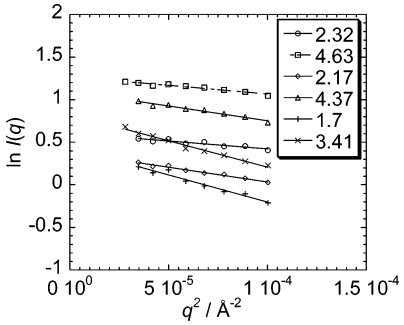

Figure 5. Guinier representations, ln $I(q)$ versus q^2/Å^{-2} for C3Ms of $P2MVP_{209}$ and PAA_{42}-*b*-$PAAm_{97}$ (○, $C_p = 2.32$ g L^{-1}; □, $C_p = 4.63$ g L^{-1}), $P2MVP_{209}$ and PAA_{42}-*b*-$PAAm_{208}$ (◇, $C_p = 2.17$ g L^{-1}; △, $C_p = 4.37$ g L^{-1}), and $P2MVP_{209}$ and PAA_{42}-*b*-$PAAm_{97}$ (+, $C_p = 1.70$ g L^{-1}; ×, $C_p = 3.41$ g L^{-1}). Used q-range is $0.005 < q < 0.01$ Å^{-1}. The first four to five points were discarded as they lack statistics and/or exhibit upturns resulting from a small fraction of aggregates in the system.

Table 1. Guinier Analysis for C3Ms of $P2MVP_{209}$ and PAA_{42}-*b*-$PAAm_N$[a]

N_{PAAm}	C_p/g L^{-1}	R_{gu}/nm	R/nm	I_0/cm^{-1}	R_{gu}/R_h
97	2.32	7.52	9.70	1.84	0.52
97	4.63	7.88	10.17	3.56	0.54
208	2.17	10.18	13.14	1.46	0.50
208	4.37	10.23	13.20	3.00	0.51
417	1.7	13.83	17.85	1.54	0.68
417	3.41	13.62	17.58	2.29	0.67

[a] $N_{PAAm} = 97$: $C_p = 2.32$ g L^{-1} and 4.63 g L^{-1}. $N_{PAAm} = 208$: $C_p = 2.17$ g L^{-1} and 4.37 g L^{-1}. $N_{PAAm} = 417$: $C_p = 1.70$ g L^{-1} and 3.41 g L^{-1}. Guinier representations are given in Figure 5. The hard sphere radius, R, has been calculated from the Guinier radius, R_{gu}, according to $R = \sqrt{5/3}R_{gu}$. R_{gu}/R_h has been calculated using the R_h as determined from the LS-T, i.e., R_h has been assumed to be independent of concentration. We estimate the uncertainties in R, R_{gu}, R_h, and I_0 to be in the order of 10%.

Clearly, for constant N_{PAAm}, scattering curves of different C_p superimpose in the high q-regime ($q > 0.02$ Å^{-1}) after division by C_p, indicating that concentration hardly affects micellar shape on these length scales (<15 nm according to π/q).

Porod representations of the scattering curves (Figure S1, see Supporting Information) reveal a Porod regime for $N_{PAAm} = 97$ and 208, but for $N_{PAAm} = 417$ no horizontal plateau is observed as it has shifted to values of q where the signal-to-noise ratio is too low, i.e., the Porod regime has disappeared into the background. As observed in Figure 4, the scattering curves superimpose in the high q-regime in all three systems after division by C_p, indicating that concentration hardly affects micellar structure on small length scales (down to ~5 nm according to π/q).

Guinier Analysis. Guinier extrapolations (Figure 5) have been performed on the two lowest concentrations of each series, to be sure that interparticle interactions were negligible. Results are given in Table 1.

As expected, we find an increase in the Guinier radius, R_{gu}, with increasing block length of PAAm, N_{PAAm}. The values for R_{gu}/R_h are very low, i.e., below the theoretical value of 0.775 for homogeneous hard spheres.[18] Still, comparably low values have been observed previously for spherical polymeric micelles.[19] Furthermore, we note that R_{gu} may be underestimated due to little shell scattering, i.e., particle scattering will be dominated by the micellar core, as the contrast between shell and solvent is much smaller than the contrast between core and shell, as the core is likely solvated up to ~50%, while the shell is likely solvated up to ~90%. Moreover, the R_h may be slightly overestimated due to the presence of a small fraction of larger aggregates, which causes visible upturns in the first few points of the scattering curves.

Table 2. Comparison of GIFT Analysis, Guinier Analysis, and Model Fitting for C3Ms of PAA_{42}-*b*-$PAAm_{97}$ and $P2MVP_{209}$

C_p/g L^{-1}	R_g[a]/nm	R_g/R_h	R_{gu}[b]/nm	R_{gu}/R_h	$\langle R\rangle$[c]/nm	$\langle R\rangle/R_h$
2.32	8.16	0.56	7.52	0.52	9.8	0.68
4.63	8.38	0.58	7.88	0.54	9.8	0.68
9.54	7.90	0.55			9.8	0.68
15.16	7.82	0.54			9.8	0.68
25.0	8.02	0.55			9.8	0.68
38.24	8.71	0.60			9.6	0.66

[a] Obtained from GIFT analysis. [b] Obtained from Guinier analysis. [c] Obtained from model fitting as described below. (We estimate the uncertainties in R_g, $\langle R\rangle$, R_{gu}, and R_h to be in the order of 10%).

Generalized Indirect Fourier Transformation. From the block length ratios, one may anticipate a spherical shape for the C3Ms of $P2MVP_{209}$ and PAA_{42}-*b*-$PAAm_N$ ($N_{PAAm} = 97$, 208, and 417). To test the validity of this assumption and to serve as a basis for further model fitting, $p(r)$ functions were computed for C3Ms of $P2MVP_{209}$ and PAA_{42}-*b*-$PAAm_{97}$ (Figure 6) using generalized indirect Fourier transformation employing the GIFT software package.[13−15] A hard sphere structure factor (Percus−Yevick closure) has been included to describe the scattering curves of the three higher concentrations.

The agreement between the experimental data and GIFT results is excellent for all samples and results in a very symmetrical shape of the $p(r)$ function typical for spherical particles.[11] The $p(r)$ curves are nearly congruent, i.e., concentration has little effect on the particle shape and structure for 2.32 g L^{-1} ≤ C_p ≤ 38.24 g L^{-1}. Hence, we conclude that the GIFT results justify model fitting with a form factor for spherical particles.

We can obtain the radius of gyration, R_g, from the GIFT results in the following manner[12]

$$R_g^2 = \frac{1}{2}\frac{\int_0^{D_{max}} p(r) r^2 \, dr}{\int_0^{D_{max}} p(r) \, dr} \tag{8}$$

Table 2 compares the radii and R/R_h values obtained through GIFT, Guinier analysis, and model fitting (see detailed description below) for C3Ms of PAA_{42}-*b*-$PAAm_{97}$ and $P2MVP_{209}$. In all cases, R/R_h values are rather low and consistent with spherical micelles with a non-negligible core.[20−22] Harada et al. have reported R_g/R_h values of 0.739−0.762 for C3Ms of poly(α,*β*-aspartic acid)-*b*-poly(ethylene oxide), PAsp-*b*-PEO, and poly((L)-lysine)-*b*-poly(ethylene oxide), PLys-*b*-PEO, or poly((L)-lysine), PLys.[23]

Model Fitting. To minimize the number of adjustable parameters, we selected the simplest possible model for polydisperse spherical particles. Thus, we apply a form factor for homogeneous spheres and a Gaussian ($N_{PAAm} = 97$ and 208) or Schulz−Zimm distribution ($N_{PAAm} = 417$) in combination with a hard sphere structure factor (Percus−Yevick closure) for the higher concentrations. Equations are given in the materials and methods sections (eqs 2−7) and in the Supporting Information (eqs S1−S15). Instrumental resolution is taken into account by applying the following equation

$$p_{real}^2 = p_{exp}^2 - p_{app}^2 \tag{9}$$

which is exact for a Gaussian (size) distribution and approximate for a Schulz−Zimm (size) distribution. Hence, the "real" polydispersity, p_{real}, is obtained when the experimentally

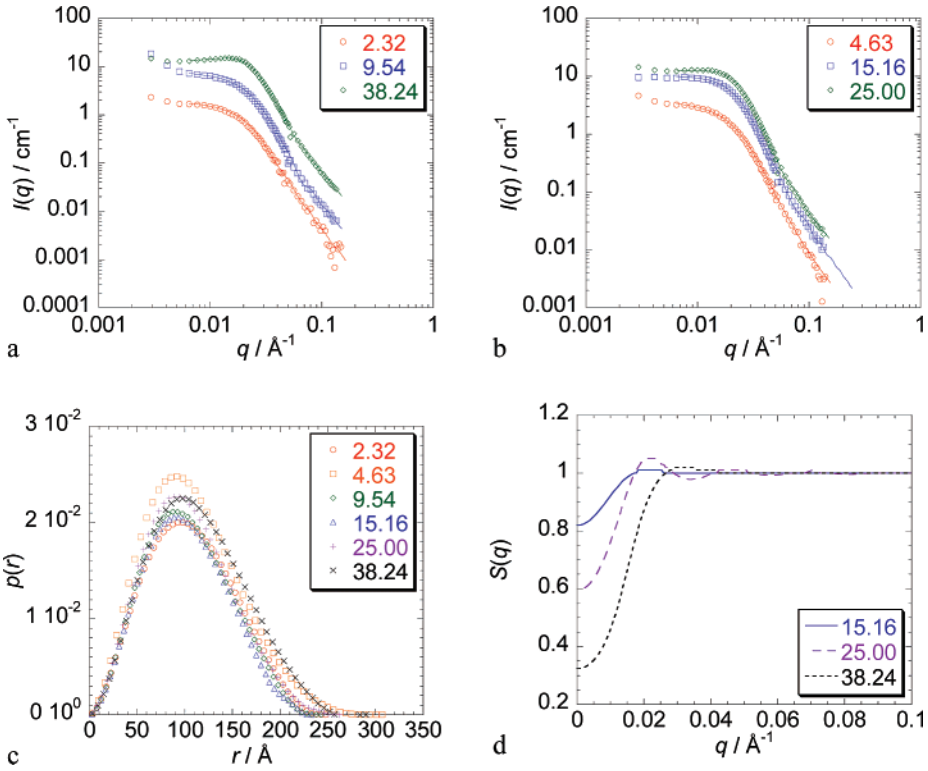

Figure 6. Results of a GIFT analysis for C3Ms of P2MVP$_{209}$ and PAA$_{42}$-*b*-PAAm$_{97}$ (2.32 g L^{-1} ≤ C_p ≤ 38.24 g L^{-1}). (a, b) $I(q)$/cm^{-1} versus q/Å^{-1}. The scattering curves were corrected for incoherent scattering due to solvent and hydrogenated polymer segments and divided by C_p. Markers correspond to experimental data; solid lines represent GIFT results. (c) $p(r)$ versus r/Å. Curves have been divided by C_p and normalized to a total area of 1; i.e., curves should superimpose in case particle shape and structure are independent of concentration. (d) $S(q)$ versus q/Å^{-1} as obtained by employing a hard sphere structure factor (Percus−Yevick closure). Results are given in Table 3. Used q-range is 0.006 < q < 0.18−0.24 Å^{-1}. The first six points were discarded as they lack statistics and/or exhibit upturns resulting from a small fraction of aggregates in the system. The used maximum distance, D_{max}, ranged from 23−31 nm.

Table 3. Model Fitting Results for C3Ms of P2MVP$_{209}$ and PAA$_{42}$-*b*-PAAm$_{97}$ (2.32 g L^{-1} ≤ C_p ≤ 38.24 g L^{-1}), PAA$_{42}$-*b*-PAAm$_{208}$ (2.17 g L^{-1} ≤ C_p ≤ 35.12 g L^{-1}), and PAA$_{42}$-*b*-PAAm$_{417}$ (1.70 g L^{-1} ≤ C_p ≤ 27.53 g L^{-1})[a]

N_{PAAm}	C_p/g L^{-1}	I_{incoh}/cm^{-1}	⟨R⟩/nm	I_0/cm^{-1}	M_{part}/ kg mol^{-1}	P_{agg}	$P_{agg,PVP}$	$\varphi_{bb,part}$	p_{real}	R_{HS}/ nm	φ_{HS}	$R_{HS,G}$[b]/ nm	$\varphi_{HS,G}$[b]
97	2.32	0.004	9.8	1.8	679	44.9	9.0	0.013	0.22				
	4.63	0.006	9.8	3.6	680	45.0	9.0	0.013	0.22				
	9.54	0.012	9.8	7.5	688	45.5	9.1	0.013	0.22				
	15.16	0.017	9.8	11.9	686	45.4	9.1	0.013	0.22	14.5	0.02	14.5	0.03
	25.00	0.027	9.8	19.9	696	46.0	9.3	0.012	0.23	14.5	0.07	13.4	0.07
	38.24	0.041	9.6	27.2	622	41.1	8.3	0.011	0.23	13.0	0.10	11.4	0.15
208	2.17	0.003	11.9	1.34	534	23.0	4.6	0.004	0.25				
	4.37	0.006	12.0	2.77	548	23.6	4.7	0.004	0.25				
	8.68	0.011	11.9	5.58	556	23.9	4.8	0.005	0.25				
	8.85	0.011	11.8	5.36	524	22.6	4.5	0.005	0.25				
	14.18	0.017	11.9	8.92	544	23.4	4.7	0.004	0.25	17.0	0.05		
	23.12	0.027	11.0	10.41	390	16.8	3.4	0.004	0.26	17.0	0.08		
	35.12	0.040	11.6	19.36	477	20.5	4.1	0.004	0.25	16.0	0.15		
417	1.70	0.004	17.1	1.40	697	18.1	3.6	0.023	0.49				
	3.41	0.009	16.5	2.26	561	14.6	2.9	0.020	0.49				
	6.89	0.015	16.5	4.56	561	14.6	2.9	0.020	0.49				
	11.01	0.021	16.5	6.79	522	13.6	2.7	0.019	0.49	16.5	0.07		
	17.91	0.034	16.5	11.05	523	13.6	2.7	0.019	0.49	16.5	0.15		
	27.53	0.052	16.5	15.47	476	12.4	2.5	0.017	0.49	16.5	0.19		

[a] The model includes a form factor for polydisperse homogeneous spheres in combination with a hard sphere structure factor (Percus−Yevick closure). A Gaussian distribution is used for N_{PAAm} = 97 and 208, and a Schulz−Zimm distribution is used for N_{PAAm} = 417. Experimental data and fits are given in Figure 7. We estimate the uncertainties in M_{part}, P_{agg}, $P_{agg,PVP}$, and $\varphi_{bb,part}$ to be in the order of 10−15%, considering standard uncertainties in their calculation, such as those in the determination of the scattering length densities (see caption of Table S1). [b] Obtained from the GIFT analysis with a hard sphere structure factor (Percus−Yevick closure, Schulz−Zimm distribution).

determined polydispersity, p_{exp} (here the result obtained from model fitting the scattering curves), is corrected for the apparent polydispersity due to a finite instrumental resolution, p_{app}.

Results are given in Figure 7 and Table 3. A global fit, i.e., keeping ⟨R⟩, p_{real}, and R_{HS} constant for a given N_{PAAm}, has been attempted but resulted in a lesser quality of fit. Still, apart from R_{HS}, the values are constant within experimental error.

As this simple model is sufficient to describe the scattering curves for all concentrations, we refrain from applying more sophisticated form factor models to the SANS data. Tests of models like, e.g., the one proposed by Pedersen[24] did not lead to a better description of the experimental data compared to the form factor for homogeneous spheres. This is mainly due to the low contrast between the heavy water and the corona.

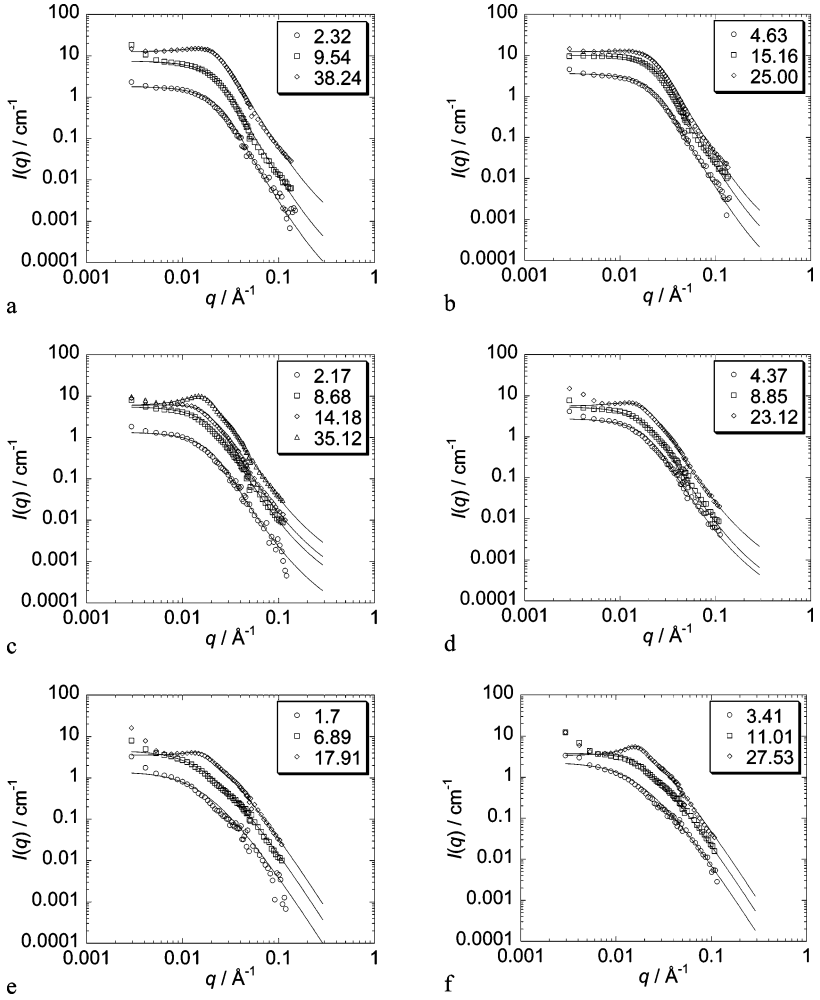

Figure 7. $I(q)/\mathrm{cm}^{-1}$ versus $q/\mathrm{Å}^{-1}$ for C3Ms of $P2MVP_{209}$ and (a, b) PAA_{42}-*b*-$PAAm_{97}$ (2.32 g $L^{-1} \leq C_p \leq$ 38.24 g L^{-1}), (c, d) PAA_{42}-*b*-$PAAm_{208}$ (2.17 g $L^{-1} \leq C_p \leq$ 35.12 g L^{-1}), and (e, f) PAA_{42}-*b*-$PAAm_{417}$ (1.70 g $L^{-1} \leq C_p \leq$ 27.53 g L^{-1}). Three concentrations are plotted per graph for reasons of clarity. Scattering curves were corrected for incoherent scattering due to solvent and hydrogenated polymer segments and divided by C_p. Markers correspond to experimental data; solid lines represent model fitting results. The model includes a form factor for polydisperse homogeneous spheres in combination with a hard sphere structure factor (Percus−Yevick closure). Used *q*-range is $0.006 < q < 0.15$ $Å^{-1}$. The first six points were discarded as they lack statistics and/or exhibit upturns resulting from a small fraction of aggregates in the system. Fit results are listed in Table 3.

Contrast variation in combination with selective deuteration is necessary to obtain information on particle internal structure, such as core and shell sizes.

As stated previously, the (polymer contribution to the) incoherent scattering, I_{incoh}, scales linearly with concentration for all three systems. In analogy to the Guinier radius, we find an increase in $\langle R \rangle$ with increasing PAAm block length, N_{PAAm}. A linear dependence of I_0 on C_p is found for a given N_{PAAm} (Figure 8) for concentrations up to 25.00, 14.18, and 17.91 g L^{-1} for $N_{PAAm} = 97$, 208, and 417, respectively. Hence, according to eq 5, we may conclude that M_{part} is concentration independent in this regime of C_p. This nicely corresponds to the conclusions drawn from the GIFT results for $N_{PAAm} = 97$. Indeed, Table 3 shows that aggregation numbers (the number of diblock copolymers, P_{agg}, and the number of $P2MVP_{209}$ polymers per micelle, $P_{agg,PVP}$) and micellar mass are nearly C_p independent for a given N_{PAAm} and decrease with increasing N_{PAAm}, as the polymer footprint (cross section) increases with increasing N_{PAAm}.

The building block volume fraction in the particle, $\varphi_{bb,part}$, calculated according to eq 7, is fairly constant at very low absolute values ($0.004 < \varphi_{bb,part} < 0.02$), which may be due to errors in the calculated scattering length densities, an underestimation of the instrumental smearing effects and/or eq 7 does not fully apply. A rather large polydispersity, increasing with increasing N_{PAAm}, is found in all three systems. We suspect it is partially stemming from the high PDI of the constituent diblock copolymers and partially intrinsic to C3Ms as they are in the so-called weak segregation limit. The latter statement is purely speculative and currently under investigation.

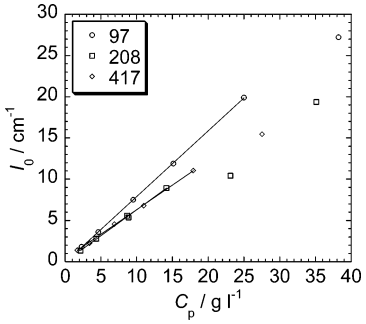

Figure 8. I_0/cm^{-1} versus C_p/g L^{-1} for C3Ms of $P2MVP_{209}$ and (○) PAA_{42}-*b*-$PAAm_{97}$, (□) PAA_{42}-*b*-$PAAm_{208}$, and (◇) PAA_{42}-*b*-$PAAm_{417}$. Values of I_0 were determined by model fitting (Figure 7, Table 3).

From the excellent agreement between experimental data and fits (Figure 7), we may conclude that a hard sphere structure factor can be used to describe C3M interparticle interaction.

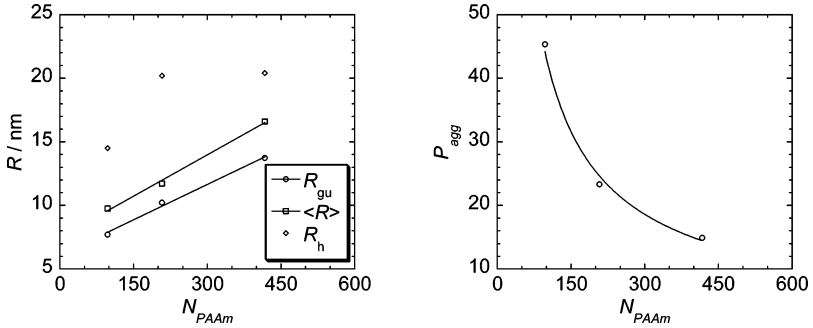

Figure 9. (a) ○, R_{gu}; □, $\langle R \rangle$; ◇, R_h and (b) P_{agg} as a function of N_{PAAm}. R_{gu}, $\langle R \rangle$, and P_{agg} values of different C_p are averaged. Lines represent linear scaling consistent with the experimental data.

However, as the particles are not hard spheres, the result is to be interpreted as an effective structure factor. The values obtained for the (effective) hard sphere interaction radius, R_{HS}, are comparable to R_h for $N_{PAAm} = 97$, while they are equal to $\langle R \rangle$ for $N_{PAAm} = 417$. As the particles become increasingly hairy and less hard spherelike with increasing N_{PAAm}, it seems reasonable that R_{HS} decreases relative to the micellar radius with increasing N_{PAAm}. Results of GIFT analysis and model fitting are fairly consistent.

Comparison with Scaling Theories. Empirically, we find a linear scaling of R_{gu} (Guinier analysis) and $\langle R \rangle$ (polydisperse sphere model) with N_{PAAm} (Figure 9a), which is a more pronounced dependence of micellar size on shell block length than predicted by scaling laws for block copolymer micelles of neutral−neutral and neutral−ionic amphiphilic polymers in any (i.e., star- or crew cut) limit.[25−29] It is likely that this deviation is partially caused by the fact that water is a very good solvent for the PAAm block, while most scaling theories suppose Θ-conditions for the shell forming block. Similarly, the power law scaling of P_{agg} with N_{PAAm} (exponent = −0.77, Figure 9b) is also more pronounced than predicted by these scaling theories, although the deviation is smaller.

Conclusions

C3Ms of $P2MVP_{209}$ and PAA_{42}-*b*-$PAAm_N$ block copolymers of varying PAAm block length (N_{PAAm} = 97, 208, and 417) have been studied by light and small angle neutron scattering. From LS-T experiments, the preferred micellar composition, PMC, was determined to be $f_+ = 0.5$ for all three systems, while the hydrodynamic radius, R_h, was found to increase with increasing N_{PAAm}. SANS experiments have been analyzed in three independent ways, namely, by generalized indirect Fourier transformation, Guinier extrapolation, and model fitting. All C3Ms reported in this paper are spherical in shape and have a considerable polydispersity ($p_{real} \geq 0.24$). Micellar aggregation numbers, shape, and internal structure are relatively independent of concentration for $C_p < 38.24$ g L^{-1}. The Guinier radius, R_{gu}, and average micellar radius, $\langle R \rangle$, were both found to increase linearly with increasing N_{PAAm}, which is a more pronounced dependence of micellar size on N_{PAAm} than predicted by scaling theories for block copolymer micelles. Micellar mass and aggregation number were found to decrease with increasing N_{PAAm}.

Acknowledgment. This work has been carried out in the framework of the EU Polyamphi/Marie Curie program (FP6-2002, Proposal 505027). One of us was financed by the SONS Eurocores program (Project JA016-SONS-AMPHI).

Supporting Information Available: Equations for the form factor for homogeneous spheres and a Gaussian or Schulz−Zimm distribution in combination with a hard sphere structure factor, overview of the coherent scattering length densities, ρ, specific volume, υ_0, and molecular weights, M_w, of the studied species, and Porod representations of the scattering curves. This material is available free of charge via the Internet at http://pubs.acs.org.

References and Notes

(1) van der Burgh, S.; de Keizer, A.; Cohen Stuart, M. A. *Langmuir* **2004**, *20*, 1073−1084.
(2) Sanson, N.; Bouyer, F.; Gerardin, C.; In, M. *Phys. Chem. Chem. Phys.* **2004**, *6*, 1463−1466.
(3) Berret, J. F.; Yokota, K.; Morvan, M.; Schweins, R. *J. Phys. Chem. B* **2006**, *110*, 19140−19146.
(4) Berret, J. F.; Vigolo, B.; Eng, R.; Herve, P.; Grillo, I.; Yang, L. *Macromolecules* **2004**, *37*, 4922−4930.
(5) Berret, J. F. *J. Chem. Phys.* **2005**, 123.
(6) Berret, J. F.; Yokota, K.; Morvan, M. *Soft Mater.* **2004**, *2*, 71−84.
(7) van der Burgh, S.; Fokkink, R.; de Keizer, A.; Cohen Stuart, M. A. *Colloids Surf., A* **2004**, *242*, 167−174.
(8) Voets, I. K.; de Vos, W.; Hofs, B.; de Keizer, A.; Cohen Stuart, M. A.; Steitz, R.; Lott, D. Submitted to *J. Phys. Chem. B.*
(9) Taton, D.; Wilczewska, A. Z.; Destarac, M. *Macromol. Rapid Commun.* **2001**, *22*, 1497−1503.
(10) Voets, I. K.; de Keizer, A.; Cohen Stuart, M. A.; Justynska, J.; Schlaad, H. *Macromolecules* **2007**, *40*, 2158−2164.
(11) Glatter, O.; Kratky, O. *Small-Angle X-ray Scattering*; Academic Press: London, U.K., 1982.
(12) Lindner, P.; Zemb, T. *Neutron, X-rays and Light: Scattering Methods Applied to Soft Condensed Matter*; Elsevier: Amsterdam, The Netherlands, 2002.
(13) Bergmann, A.; Fritz, G.; Glatter, O. *J. Appl. Crystallogr.* **2000**, *33*, 1212−1216.
(14) Weyerich, B.; Brunner-Popela, J.; Glatter, O. *J. Appl. Crystallogr.* **1999**, *32*, 197−209.
(15) Glatter, O. *J. Appl. Crystallogr.* **1977**, *10*, 415−421.
(16) Percus, J. K.; Yevick, G. J. *Phys. Rev.* **1958**, *110*, 1−13.
(17) Brunner-Popela, J.; Glatter, O. *J. Appl. Crystallogr.* **1997**, *30*, 431−442.
(18) Konishi, T.; Yoshizaki, T.; Yamakawa, H. *Macromolecules* **1991**, *24*, 5614−5622.
(19) Qin, A. W.; Tian, M. M.; Ramireddy, C.; Webber, S. E.; Munk, P.; Tuzar, Z. *Macromolecules* **1994**, *27*, 120−126.
(20) Vagberg, L. J. M.; Cogan, K. A.; Gast, A. P. *Macromolecules* **1991**, *24*, 1670−1677.
(21) Mossmer, S.; Spatz, J. P.; Moller, M.; Aberle, T.; Schmidt, J.; Burchard, W. *Macromolecules* **2000**, *33*, 4791−4798.
(22) Zhang, W. A.; Zhou, X. C.; Li, H.; Fang, Y.; Zhang, G. Z. *Macromolecules* **2005**, *38*, 909−914.
(23) Harada, A.; Kataoka, K. *Macromolecules* **2003**, *36*, 4995−5001.
(24) Pedersen, J. S.; Gerstenberg, M. C. *Macromolecules* **1996**, *29*, 1363−1365.
(25) Halperin, A. *Macromolecules* **1987**, *20*, 2943−2946.
(26) Noolandi, J.; Hong, K. M. *Macromolecules* **1983**, *16*, 1443−1448.
(27) Nagarajan, R.; Ganesh, K. *J. Chem. Phys.* **1989**, *90*, 5843−5856.
(28) Dan, N.; Tirrell, M. *Macromolecules* **1993**, *26*, 4310−4315.
(29) Zhulina, E. B.; Adam, M.; LaRue, I.; Sheiko, S. S.; Rubinstein, M. *Macromolecules* **2005**, *38*, 5330−5351.

MA071356Z